Accepted Manuscript

Microstructural evolution and mechanical properties of maraging steel produced by wire+arc additive manufacture process

Xiangfang Xu, Supriyo Ganguly, Jialuo Ding, Shun Guo, Stewart Williams, Filomeno Martina

PII: S1044-5803(17)32757-2
DOI: doi:10.1016/j.matchar.2017.12.002
Reference: MTL 8951

To appear in: *Materials Characterization*

Received date: 15 October 2017
Revised date: 29 November 2017
Accepted date: 3 December 2017

Please cite this article as: Xiangfang Xu, Supriyo Ganguly, Jialuo Ding, Shun Guo, Stewart Williams, Filomeno Martina , Microstructural evolution and mechanical properties of maraging steel produced by wire+arc additive manufacture process. The address for the corresponding author was captured as affiliation for all authors. Please check if appropriate. Mtl(2017), doi:10.1016/j.matchar.2017.12.002

Materials Characterization, Volume 143, September 2018, Pages 152-162
DOI:10.1016/j.matchar.2017.12.002

Microstructural evolution and mechanical properties of maraging steel produced by wire + arc additive manufacture process

Xiangfang Xu[a,1], Supriyo Ganguly[a], Jialuo Ding[a], Shun Guo[b], Stewart Williams[a], Filomeno Martina[a]

[a] Welding Engineering and Laser Processing Centre, Cranfield University, Bedford, MK43 0AL, UK

[b] School of Materials Science and Engineering, Nanjing University of Science and Technology, Nanjing, 210094, China

Abstract: Wire + arc additive manufacture is developed for producing large-scale metallic components. In this paper, maraging steel parts were produced, and the microstructure and mechanical properties were investigated. The microhardness and tensile strength of the as deposited alloy reduced from the bottom to the top due to the transient thermal cycling, which resulted in partial aging and non-uniform formation of intermetallic compounds along the building direction. Solutionizing, followed by 3 hours aging, significantly reduced the microstructural heterogeneity and increased the mechanical properties by 24.7% through the formation of large amounts of finely distributed precipitates. The as deposited alloy possessed superior strength to the wrought alloy in solutionized condition but inferior to the later in aged condition, which was attributed to the less pronounced aging response of the low-angle columnar grains characterized microstructure and the presence of retained and reverted austenite.

Keywords: wire + arc additive manufacture; maraging steel; precipitates; mechanical properties; heat treatment

[1] Corresponding author.
Phone: +44-7951958136
E-mail address: xiangfang.xu@cranfield.ac.uk (X. Xu).

[1] Corresponding author.
E-mail address: xiangfang.xu@cranfield.ac.uk (X. Xu).

Microstructural evolution and mechanical properties of maraging steel produced by wire + arc additive manufacture process

1. Introduction

Wire + arc additive manufacture (WAAM) has been developed for the fabrication of large-scale (meter scale) metallic structures for advanced applications [1,2]. In this process, an electric arc is used as the heat source and the commercial welding wire is used as the feedstock material [3]. Usually, a pre-programed robot arm is deployed to control the movement of the deposition path in a layer-by-layer manner to manufacture full-dense functional components. The feasibility of WAAM process has been verified by various materials ranging from titanium [4], aluminium [5,6], steel [7] to inconel [8]. Compared with other existing additive manufacturing (AM) process, WAAM is characterized by low equipment cost, high deposition rate, reduced lead time and large-scale and full density parts [9].

Maraging steels are developed to combine superior high strength (yield strength commercially ranging from 1030 to 3450 MPa) with good fracture toughness [10]. The absence of carbon makes maraging steels different from conventional steels in that they are strengthened by the intermetallic compounds precipitated from the supersaturated martensite during the age hardening of the ductile low-carbon iron-nickel lath martensitic matrix [11]. In the solutionized condition, maraging steels are relatively soft with excellent machinability and weldability; a subsequent aging heat treatment can significantly improve the strength. Due to the low coefficient of expansion of maraging steel, the size change after aging is negligible (e.g. 0.0009 inch/inch for 250-grade maraging steel). The combination of these advantages makes maraging steels attractive for different sectors such as aircraft, aerospace [12], die-casting, tooling and weapon applications.

The maraging steels gain optimum mechanical properties through an aging heat treatment. However, due to the very small size (nanometre scale) and coherent distribution of these precipitates and the complex alloying system in maraging steel, there have long been a lack of effective characterization methods and a great deal of discussion on the strengthening mechanism [13]. The prevailing idea is that Mo acts as the primary hardener by forming ribbon-shaped Ni_3Mo and Ti serves as the secondary hardener through the formation of spherical-shaped Ni_3Ti. Further aging is reported to cause the in situ transformation from the metastable Ni_3Mo to the equilibrium Fe_2Mo. Fe_7Mo_6 is another precipitate that is often reported [14]. Cobalt does not precipitate as it does not form precipitates with Fe, Ni, Mo and Ti, but it reduces the solubility of Mo in the Fe-Ni alloys, thus increasing the amount of Ni_3Mo formed during aging [15].

So far, only a few attempts have been made with selective laser melting (SLM) process to additively manufacture maraging steel parts [16–19]. The ultimate tensile strength (UTS) of maraging steel

produced by SLM are comparable to the wrought alloy in aged condition: 2094 MPa [19] and 2217 MPa [20] of SLM 300-grade maraging steel compared to 2050 MPa of wrought alloy of the same grade. However, the SLM process is featured with low deposition rate due to the size of the powder used (normally a few to a few hundred micrometers). Besides, due to the fast scanning speed and cooling rate in SLM, unmelted powder particles were found trapped in the additively manufactured parts as inclusions [17]. Full density is not always guaranteed (relative density ranging from 90.9% to 99.9% [19]) as a result of the unmelted particles and oxides inclusions, which adversely affected the mechanical properties of the AM parts [21]. As reported [18], the SLM processed alloy showed a reduced toughness of 30-40% in the aged condition.

The aging temperature of maraging steel is relatively low (482°C) and will be frequently passed during the repeating melting-cooling deposition process, causing some extent aging effect. However, this transient aging is quite different from the conventional artificial aging where the components are deliberately kept at a certain temperature and hold for some duration. In addition, the aging response depends on the microstructure. In contrast to the wrought alloy where the whole part undergoes uniform thermal processing, different layer of the AM component goes through different numbers of thermal cycles based on the deposition sequence and the design of deposition. Therefore, when manufacturing a component by AM, different microstructure and mechanical properties can be expected from the conventional wrought route alloy.

Until now, few researches have been carried out to apply arc based AM process to manufacturing maraging steel components. The present research is aimed at understanding the application of WAAM process to produce maraging steel structures. Microstructural evolution, phase transformation and its effect on the aging response have been investigated and correlated to the mechanical properties of the WAAM products.

2. Materials and methods

The WAAM system in the present research mainly consisted of a six-axis FANUC robot, a plasma power source, a plasma torch, an external wire feeder and a working platform, as shown in Fig. 1. The entire setup was placed in an enclosure filled with pure argon gas and the oxygen level was controlled below 500 ppm through an oxygen analyser. The wire used for the study was MARVAL 18S of 1.2 mm in diameter which is designed to weld 200 and 250-grade maraging steel. The chemical composition of the wire and the wrought 250-grade maraging steel, and the nominal chemical composition of the 200-grade maraging steel are listed in Table 1. It can be seen that the chemical composition of the wire is in between the 200 and 250-grade maraging steel, yet closer to the 250-grade one.

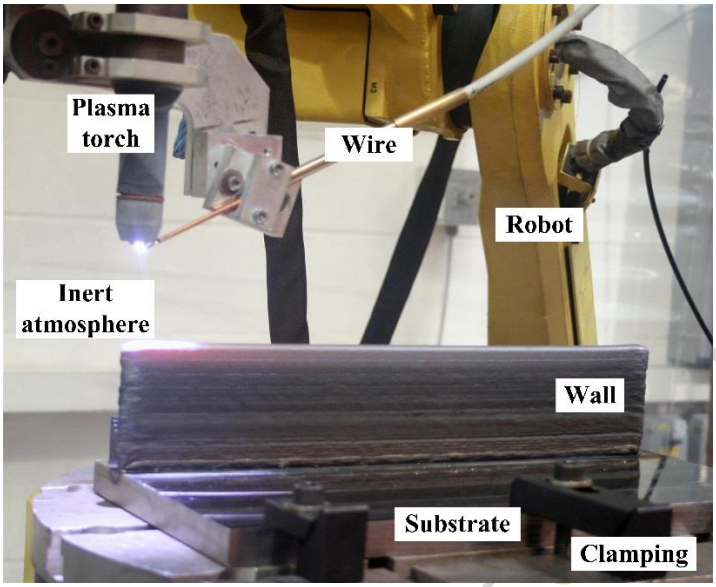

Fig. 1 Experimental setup of the WAAM system

Table 1. Chemical composition of the MARVAL 18S wire, maraging 200 and 250-grade steel (wt. %)

	Ni	Mo	Co	Ti	Al	C	Fe
Wire [a]	18.28	4.69	8.21	0.44	0.11	<0.01	Balance
18Ni (200) [15]	18	3.3	8.5	0.2	0.1	<0.03	Balance
18Ni (250) [b]	18.3	4.8-4.9	7.7	0.5	0.07-0.08	0.004	Balance

[a] *from data sheet of the wire package*

[b] *from date sheet provided by Smiths Metal Centres*

A 21-layer maraging steel linear wall structure was deposited to study the microstructural evolution of the as deposited WAAM component and its response to a standard aging heat treatment. A piece of wrought 250-grade maraging steel was also prepared following the same heat treatment procedure to investigate the microstructural difference between the maraging steels produced in two different processing routes. Subsequently, a large linear wall (dimension: 400×123×10mm) was deposited to study the mechanical properties of the maraging steel produced by WAAM. The heat treatment applied to the as deposited wall structure consists of two steps: solutionizing at 815 °C with a holding time calculated as 1 hour for every inch of thickness, air-cooling to room temperature, and then aging at 482°C for 3 hours followed by air-cooling to room temperature, as recommended by ASM handbook for 250-grade maraging steel [22].

Samples were transverse cross-sectioned from the as deposited wall for metallographic analysis, microhardness measurement and heat treatment evaluation by following a procedure consisting of mounting, grinding, polishing and etching (with 10% nital solution) successively. The microstructure was analyzed with an OLYMPUS Confocal Scanning Laser Microscope (OLS3000) and a Scanning Electron Microscope (SEM, FEI XL30-SFEG) equipped with the energy-dispersive spectrometry detector (EDS, which was also used to measure the elemental composition of the WAAM material in the research). The microhardness was measured with the Zwick/Roell Hardness Tester along the central line from the bottom (the area near the substrate) to the top of the wall structure under a load of 1 kg (holding time: 15s). The electron backscatter diffraction (EBSD) analysis was used to quantitatively analyze precipitates distribution in both as deposited and heat treated condition. Tensile test samples were prepared according to BS EN ISO 6892-1:2009 standard in a proportional design to evaluate the mechanical properties with Instron 5500R electromechanical testing machine (load cell: 100KN, crosshead speed: 1mm/min) at room temperature. The samples are painted with the graphite and then equipped with the reflective tape to measure the elongation during the tensile test (gauge length = 28mm) through the laser extensometer. Two sets of tensile coupons were taken from the WAAM wall to represent the as deposited and heat treated conditions respectively. The volume fraction of austenite was estimated by X-ray diffraction (XRD) analysis [10] using the SIEMENS D5005 diffractometer with Cu Kα radiation (λ=1.5418 Å) at room temperature. The XRD was operated at 40 kV and 40 mA with the scan rate of 0.04°/s over the 2θ range from 20 to 90°. DIFFRAC.EVA V4.1 software was used to analyse the XRD patterns.

3. Results

3.1 Microhardness and macrostructure

Fig. 2 presents the overall macrostructure of the as deposited maraging steel wall and the microhardness variation from the bottom to the top part in both as deposited and heat treated conditions. Defects, such as inclusions or porosities, are not observed in the macrostructure, indicating a fully dense as deposited WAAM part. Uniformly distributed layer bands composed of the martensitic structure with a fine dispersion of reverted austenite [23] are observed in the previously deposited layers from successive thermal cycles.

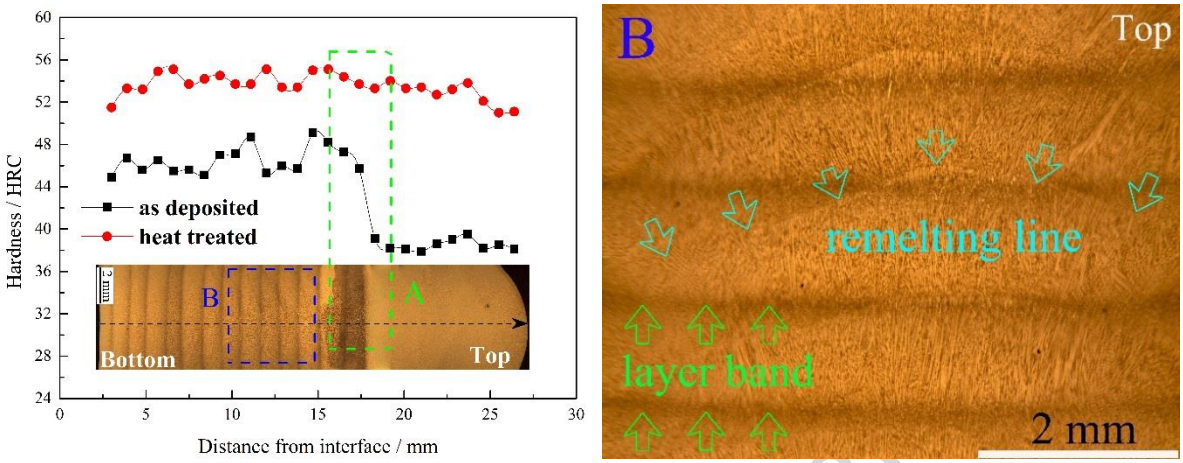

(a) microhardness measurements (b) enlarged Zone B from Fig. 2a

Fig. 2 Microhardness measurements and macrostructure of the WAAM maraging steel

As shown in Fig. 2a, in the as deposited condition the WAAM structure is not uniform in microhardness from the bottom to the top: the material is harder (ranging from 44 to 49 HRC) in the bottom part but gets softened significantly near and above the first layer band to around 32 HRC. After heat treatment, the hardness increases to between 52 to 56 HRC and the variation from bottom to the top layers becomes less pronounced. Considering that the low-carbon iron-nickel martensite formed after solutionizing is relatively soft (around 33 HRC), it can thus be inferred that the maraging steel produced by WAAM is non-uniformly age hardened to different extents from the bottom to the top along the building direction with the bottom aged more.

3.2 Microstructure

The microstructure of the WAAM component in the as deposited and heat treated conditions is displayed in Fig. 3. A typical dendritic structure with long columnar grains is observed at the bottom part of the as deposited material which clearly displays the iron-nickel martensitic matrix decorated with austenite (shown as white pools) between the dendrites; whereas the top part is also dendritic with less columnar grains and shows less contrast after etching with little austenite observed.

As shown in Fig. 3b, after the heat treatment, the formation of a large amount of precipitates all over the WAAM structure adds to the contrast near the top part after etching. The microstructure throughout the cross section shows a greater proportion of discrete austenitic islands along the inter-dendritic boundaries. Besides, the low-carbon lath martensite becomes thinner and the aspect ratio of the austenitic islands becomes lower, transforming from dendritic shape to a more circular shape after heat treatment.

Fig. 4 shows the microstructure of the heat treated maraging steel produced by traditional wrought process. Different from the dendritic microstructure of the WAAM product, the microstructure of the wrought maraging steel is characterized by equiaxed grains with the average grain size of around 30 μm. Such microstructural difference is due to the thermal extraction orientation and uniformity during the solidification process: for a linear wall structure produced by WAAM, the heat is extracted preferentially from the top to the bottom and the thermal conduction is constrained along the wall-thickness direction, which facilitates the columnar grains formation; while in the traditional wrought process, the thermal conduction is uniformly in all directions, which leads to the equal growth of dendrites in all directions during the crystallization process to form equaxed grains. Generally, equiaxed microstructure provides isotropic mechanical properties. It should also be highlighted that few retained austenite are observed among the lath martensitic matrix in the wrought material.

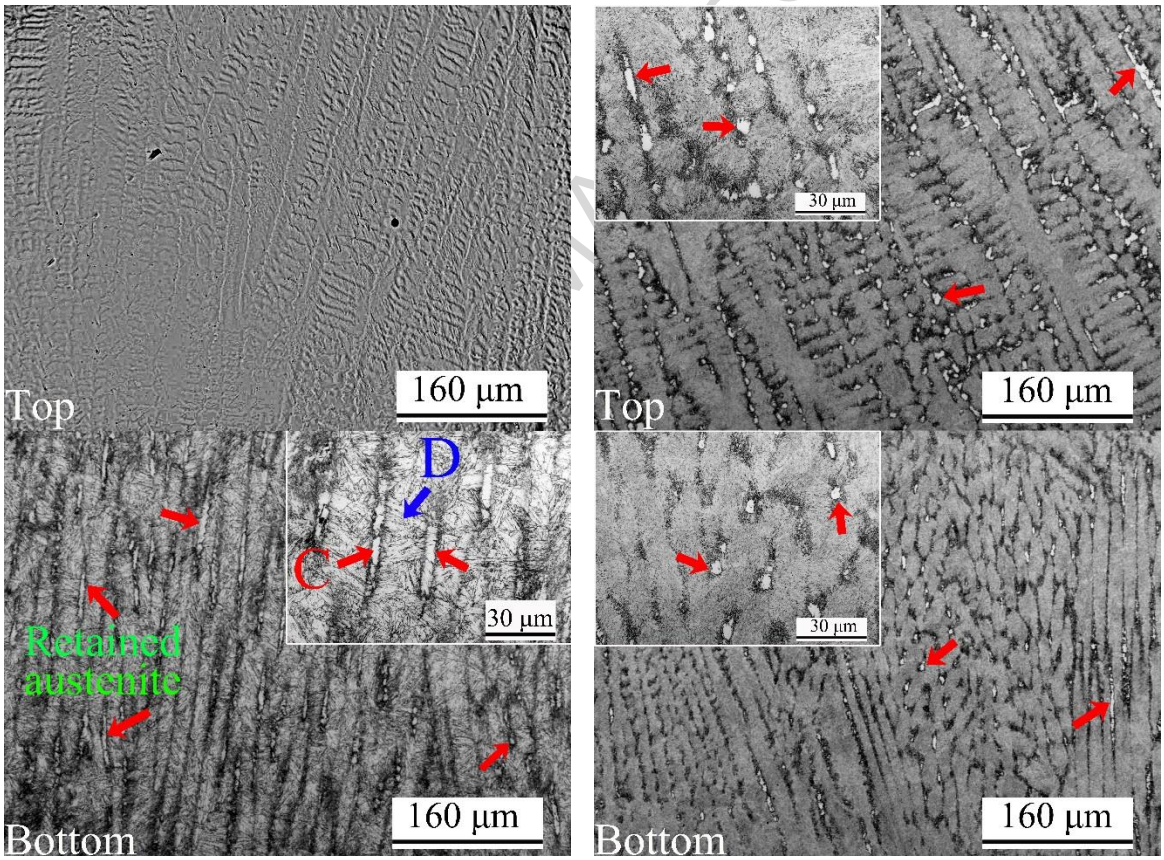

(a) as deposited (b) heat treated

Fig. 3 Microstructure of the maraging steel produced by WAAM process

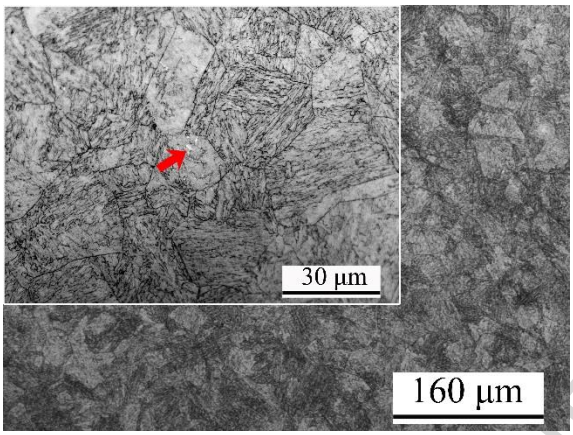

Fig. 4 Microstructure of the heat treated maraging steel produced by wrought process

Table 2 shows the EDS elemental analysis results of the austenite and martensitic matrix from Fig. 3a. As can be seen, the austenite is rich in Ti (1.39% compared to 0.44% in wire) and Mo (5.16% compared to 4.69% in wire); in comparison, the martensitic matrix in the vicinity of the austenite shows less content in Ti (0.08% to 0.44% in wire) and Mo (3.09% to 4.69% in wire). Such a Ti depleted zone could occur due to the enhanced elemental segregation caused by the austenite reversion during the deposition process. Fig. 5 presents the EDS mapping results of the austenite and its surrounding martensitic matrix, which also proves that the austenite is rich in Mo and Ti compared to the matrix. Therefore, it can also be concluded that the formation of the austenite was promoted by the element segregation, mainly Ti and Mo [27].

Table 2. EDS elemental analysis of the austenite and martensitic matrix (wt. %)

	Ti	Mo	Ni	Co	Rest (Fe, Al, C)
C	1.39	5.16	19.85	8.89	balance
D	0.08	3.09	17.41	8.38	balance
wire	0.44	4.69	18.28	8.21	balance

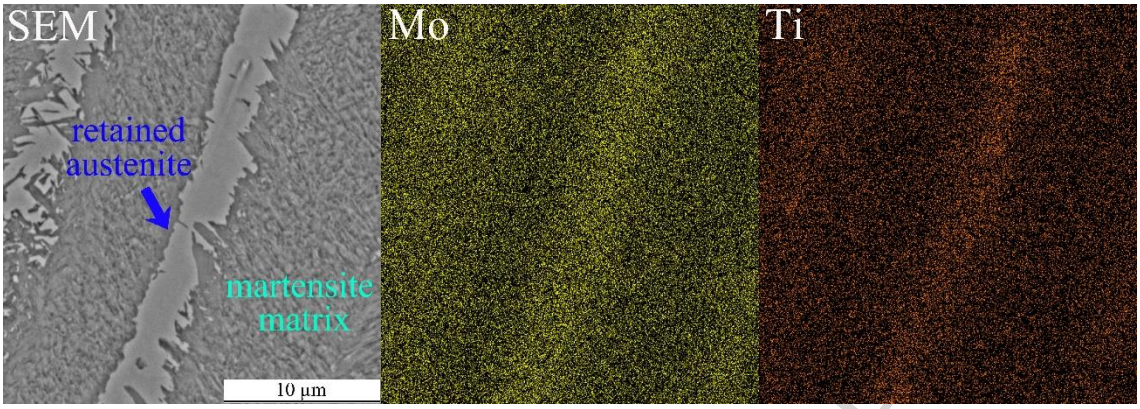

Fig. 5 EDS mapping of the austenite and the martensitic matrix

As has been reported, the austenite in maraging 250-grade steel forms when heated at 650°C or higher[28]; however, compared to the as deposited condition, larger amount of austenite forms when the WAAM built component is aged at only 482 °C (Fig. 3b), which indicates that such elemental segregation could also lower the austenite reversion temperature.

3.3 Precipitates formed in WAAM

In WAAM process, the as deposited material undergoes repeated thermal cycles from subsequent depositions and partial aging effect could occur, which has been verified by the previous hardness measurement. Fig. 6 presents the SEM results of the precipitates formed in the WAAM structure. Due to the lack of aging effect, few precipitates are found in the top part of the as deposited maraging steel; while some spherical precipitates are observed to be dispersed in the martensitic matrix near the bottom part, which is in agreement with the previous hardness measurement that the bottom part is harder than the top part. Such a microstructural heterogeneity is eliminated through a solution and a subsequent aging heat treatment, which allows controlled release of the solute atoms and formation of the uniformly distributed precipitates, as shown in Fig. 6b.

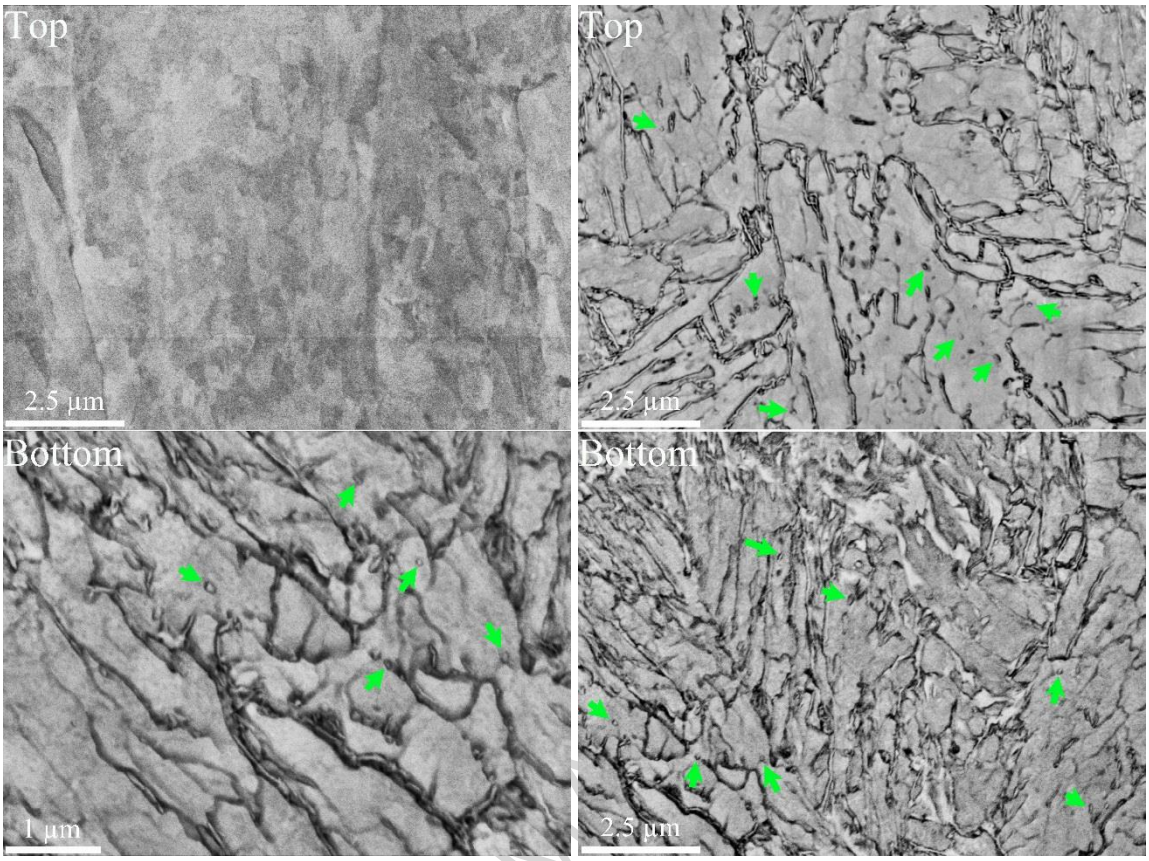

(a) as deposited (b) heat treated

Fig. 6 Precipitates in the maraging steel produced by WAAM (BSE mode)

Fig. 7 illustrates the EBSD phase mapping results of the main precipitates-Ni_3Mo, Ni_3Ti, Fe_2Mo and Fe_7Mo_6 [29–31] for the bottom and top parts in both as deposited and heat treated conditions. As has been reported, the size of these precipitates is very small (nanometre scale [13,32]). In Figs. 7a and 7b, significant amounts of the precipitates are observed in finely dispersed condition throughout the martensitic matrix, preferentially on dislocations and within the lath martensite. Fig. 7c shows the calculated content (percentage in area) of the precipitates for Figs. 7a and 7b. As can be seen, under the as deposited condition, the bottom part has larger, around twice, the amount of precipitates than the top part. After 3 hours of aging, the amount of precipitates near the top part increased significantly, Fe_2Mo from 0.0827% to 0.335%, Fe_7Mo_6 from 0.286% to 0.742%, Ni_3Mo from 0.0974% to 0.189% and Ni_3Ti from 0.0656% to 0.159%. The increase near the bottom after aging is less significant in Fe_2Mo (from 0.2195% to 0.2379%) but noticeable in Fe_7Mo_6 (from 0.523% to 0.792%), Ni_3Mo (0.217% to 0.456%) and Ni_3Ti (from 0.158% to 0.305%). Such an increase in the top part brings the amount of precipitates across the WAAM structure to almost the same level, making the heat treated WAAM part uniform in phase contents.

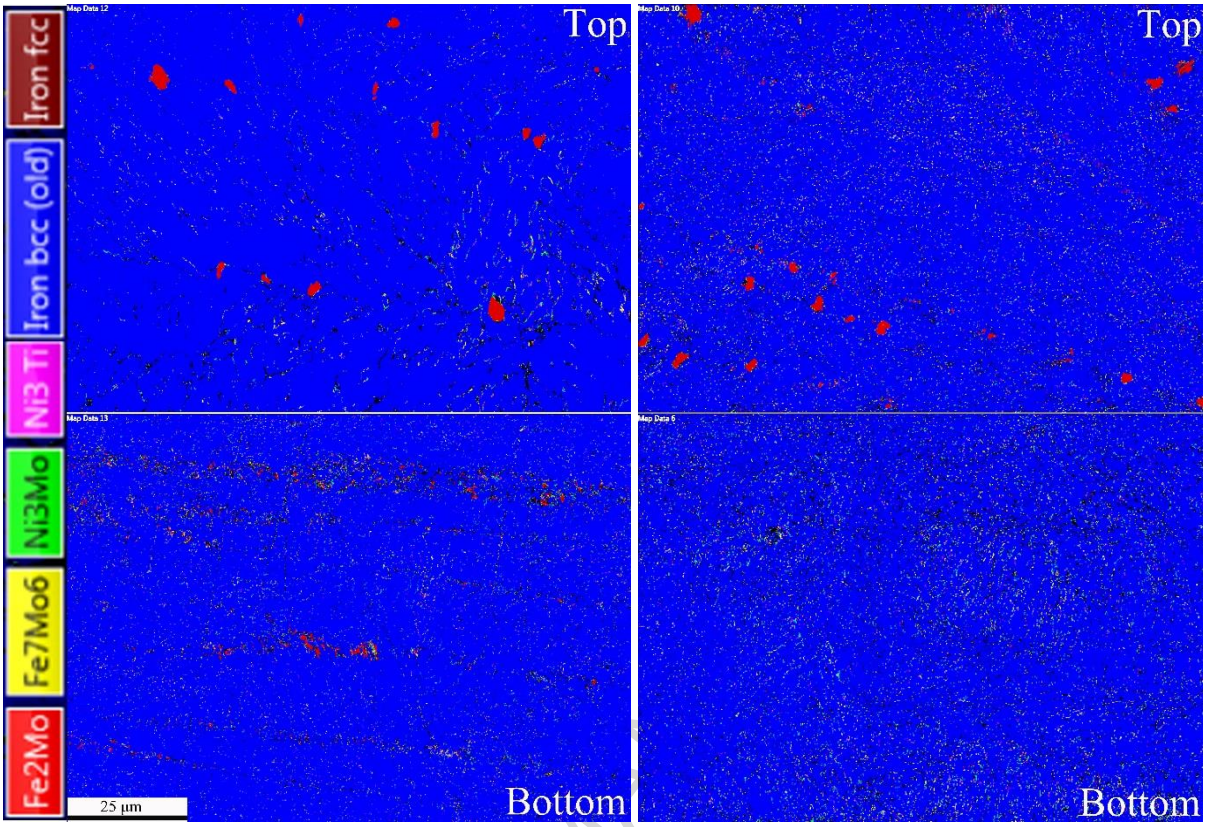

(a) as deposited (b) heat treated

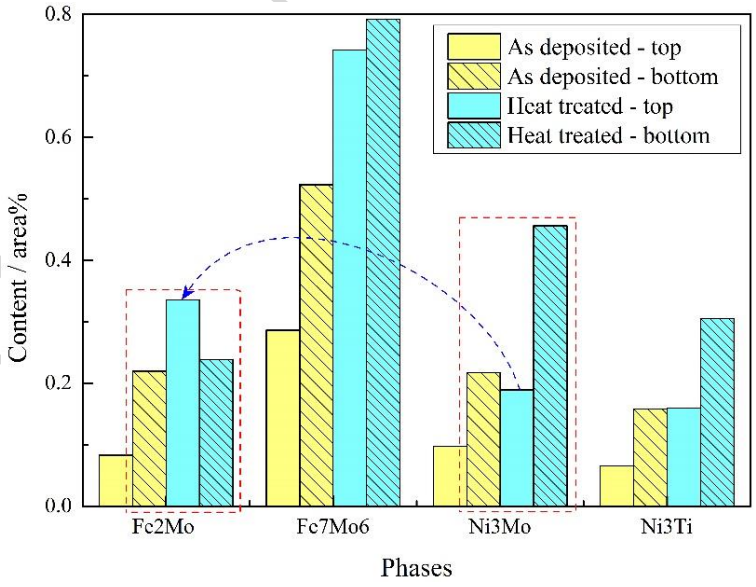

(c) content of precipitates

Fig. 7 EBSD Phases distribution

3.4 Mechanical properties

The linear wall structure for the tensile test was deposited in an alternating direction manner to make it equal heights at both ends. An effective zone is selected 15mm away from both ends and 10mm away from the substrate to eliminate the ends effects and the dilution effect from the substrate, as shown in Fig. 8a. Samples numbering according to their locations and the dog-bone drawing used in the experiment are shown in Figs. 8b and 8c, respectively.

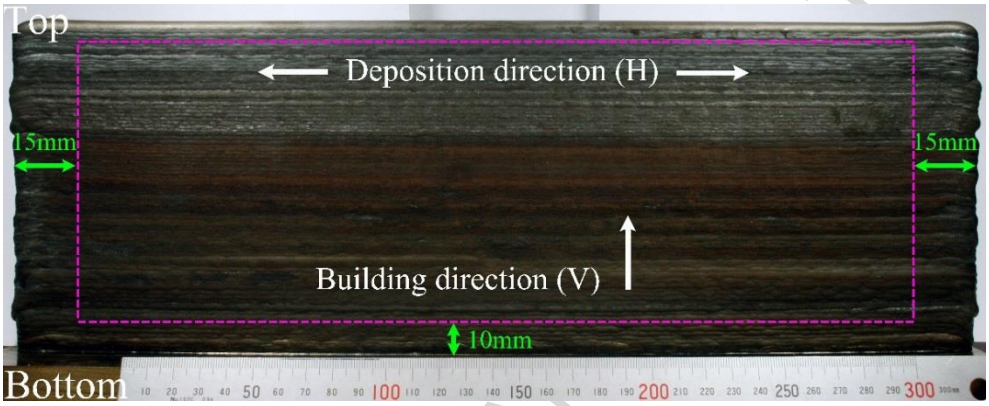

(a) as deposited maraging steel wall structure

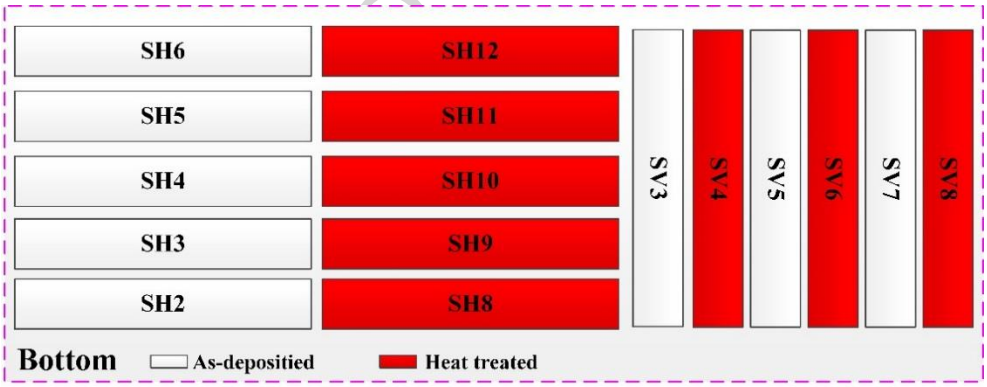

(b) samples numbering and locations

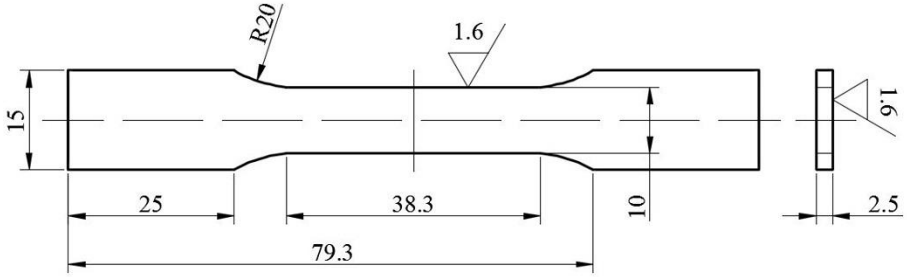

(c) dog-bone drawing

Fig. 8 Maraging steel wall for tensile test, sample numbering and dog-bone drawing

3.4.1 Testing results

Fig. 9 and Table 3 present the mechanical testing results of the maraging steel prepared by the WAAM process along both the deposition direction (Horizontal) and building direction (Vertical). In the as deposited condition, the UTS and 0.2% yield strength (0.2%YS) generally reduce from the bottom to the top: from 1282 MPa to 994 MPa and from 1048 MPa to 878 MPa, respectively, which is in line with the microhardness measurements and the phase content statistical results. However, such variation is not observed in the vertical direction. On average, the UTS and 0.2%YS in the horizontal direction are 9.0% and 8.5% higher than the vertical direction, respectively, indicating the anisotropy to some extent. This is partially due to the existence of the layer bands in the as deposited material, which reduce the tensile strength in the direction perpendicular to them. After the standard aging heat treatment, the UTS and 0.2%YS values at each corresponding locations increase noticeably, with the UTS increased by 26.1% (horizontal) and 31.1% (vertical) and the 0.2%YS increased by 44.1% (horizontal) and 47.3% (vertical). Although the anisotropy of mechanical properties is still present after heat treatment, with the UTS and 0.2%YS in the horizontal direction 4.8% and 6.2% higher than the vertical direction, the variations in UTS and 0.2%YS values from the bottom to the top are virtually eliminated. The elongation values in the as deposited condition are generally consistent in both directions with only one exception (sample SV5); after heat treatment, the scattering in elongation measurements becomes significant but in general, the elongation drops when compared to the as deposited condition. A typical comparison of the strain-stress curve of the tensile test samples in different conditions is present in Fig. 10.

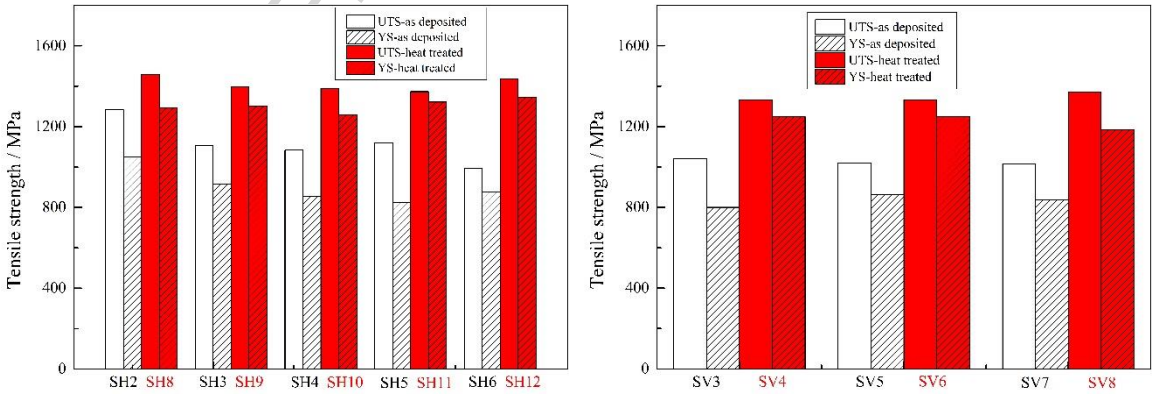

(a) tensile strength-horizontal (b) tensile strength-vertical

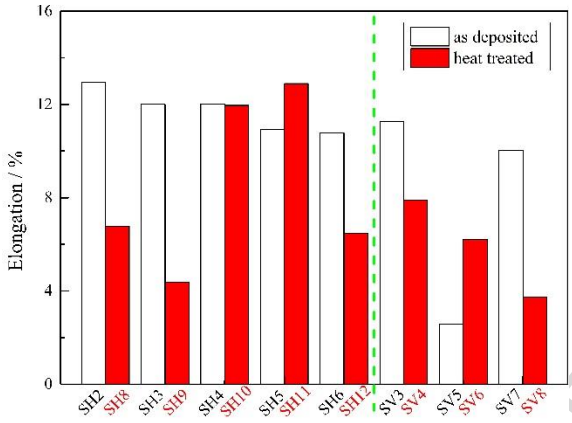

(c) elongation

Fig. 9 Mechanical testing results

Table 3. Summary of mechanical properties of maraging steel

		UTS /MPa	0.2%YS /MPa	Elongation /%
as deposited	WAAM (horizontal)	1118±94	904±78	11.7±0.8
	WAAM (vertical)	1026±10	833±26	8.0±3.8
unaged	Wrought 200 [15]	965-1000	760-807	17-18
	Wrought 250 [15]	1000-1140	725-895	8-16
aged	WAAM (horizontal)	1410±32	1303±29	8.5±3.3
	WAAM (vertical)	1345±19	1227±31	6.0±1.7
	Wrought 200 [33]	1450	1380	12
	Wrought 250 [33]	1760	1720	10

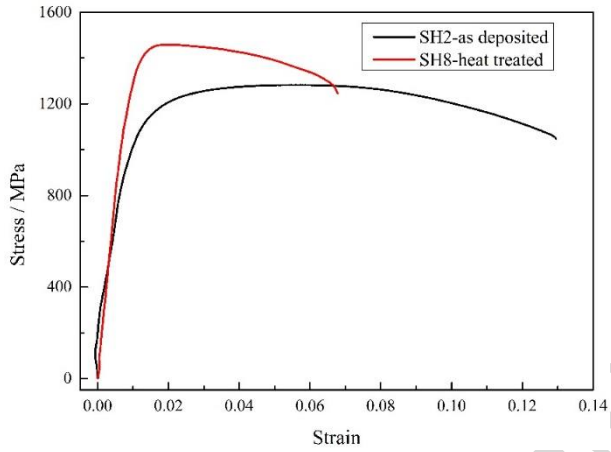

Fig. 10 Strain-stress curve

From the summary of Table 3, it should also be noticed that the mechanical properties of the maraging steel produced by WAAM in the as deposited condition are comparable, or even better than those of the unaged wrought maraging 200 and 250-grade steel regarding UTS, 0.2%PS and elongation. However, after heat treatment, the WAAM structure shows relatively lower mechanical properties than the wrought alloy, wherein the overall average UTS is 50 MPa and 360 MPa lower and the 0.2%PS is 91 MPa and 430 MPa lower than the aged 200 and 250-grade maraging steel respectively.

3.4.2 Fracture surface

Fig. 11 presents the typical fracture surfaces of the tensile test specimens. The as deposited material generally shows a ductile manner fracturing with large deformation, resulting from the micro void coalescence. In contrast, the heat treated material shows more brittle fractures in a quasi-cleavage and ductile combined manner. Dimples are found in both conditions wherein the dimples in the as deposited material are of larger amount and more uniform in size. Micro cracks are found in the heat treated material, which initiates the fast failure during the tensile test (as indicated by the yellow arrow in Fig.11b and 11d). Nano-sized pores are observed to be dispersed in both conditions with smooth inner morphology, which results from the nanosize precipitates being pulled out of the matrix during the tensile test (see pink arrow in Fig. 11c).

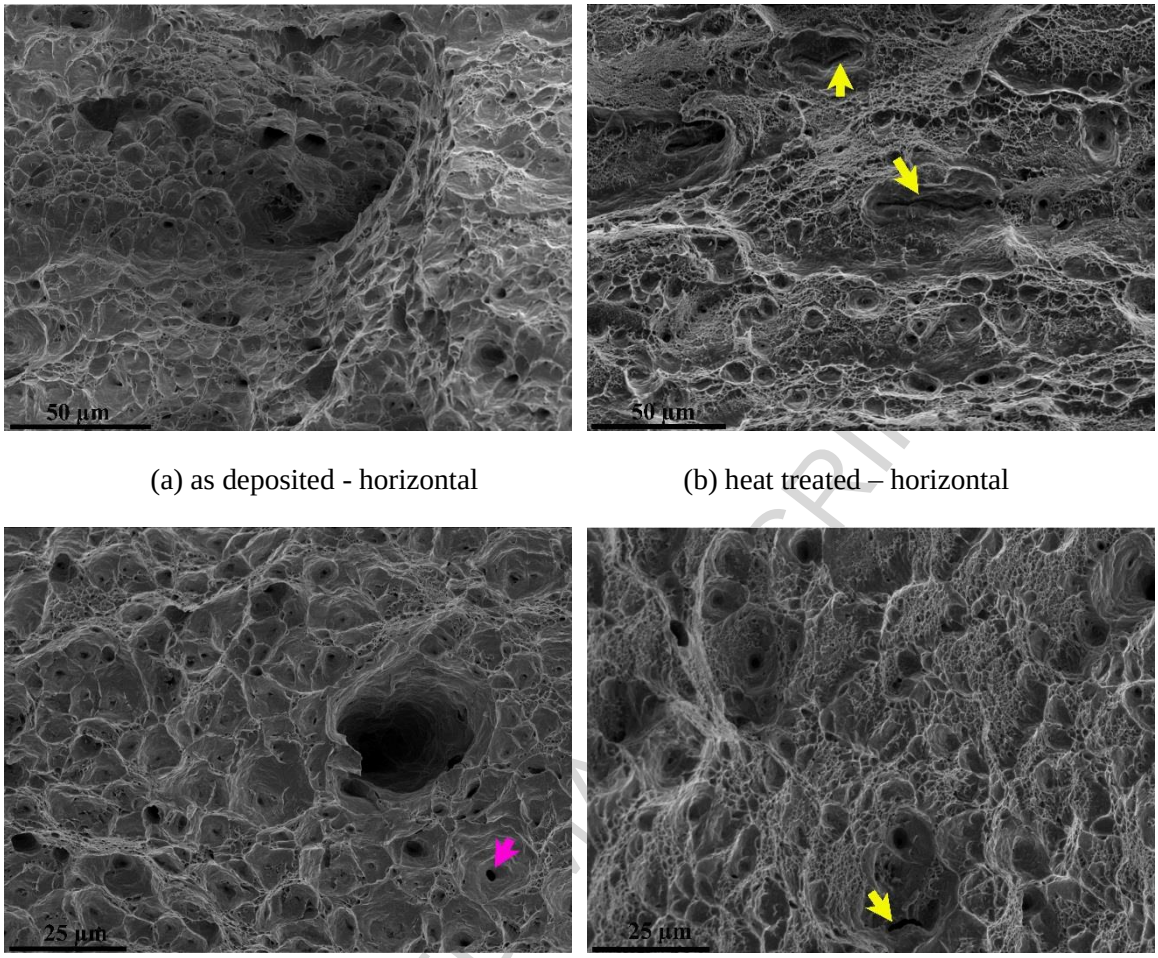

(a) as deposited - horizontal (b) heat treated – horizontal

(c) as deposited - vertical (d) heat treated - vertical

Fig.11 Fracture surface of the tensile test samples

Fig. 12 shows the optical micrographs of the joint fracture surfaces from the longitudinal section. As can be seen, the ductile fracture surface shows a typical cup and cone fracture with the shear lip 45° with respect to the base of the cup and cone, indicating the micro void coalescence happened during the tensile test. In contrast, the brittle fracture surface in the heat treated material shows a characteristic flat edge; the elongated austenites are also observed to distribute among the elongated matrix material, which is not observed in the same area in the as deposited material.

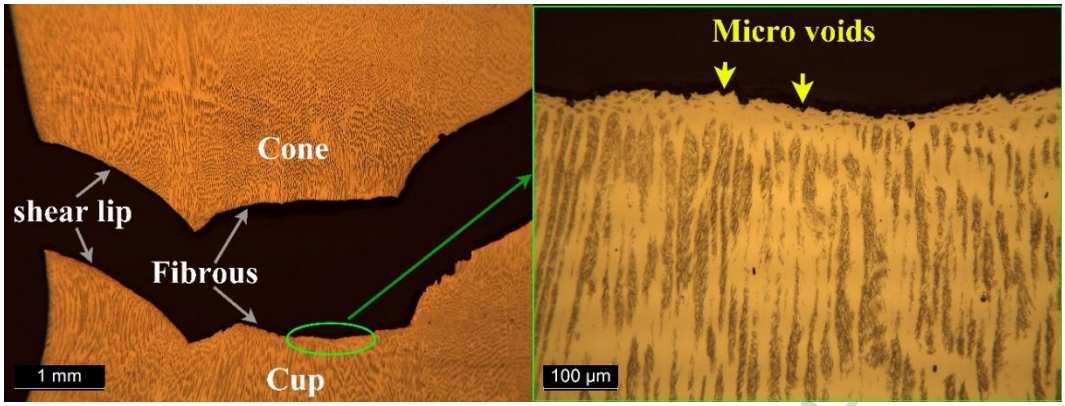

(a) as deposited

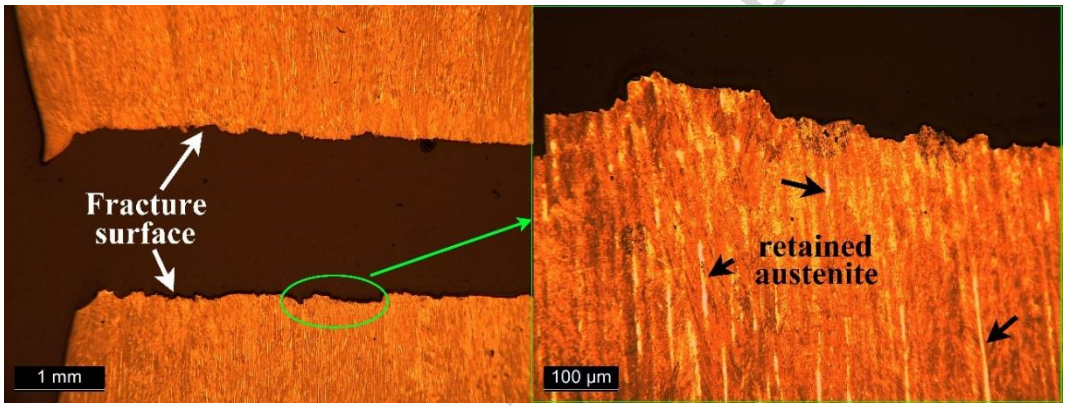

(b) heat treated

Fig. 12 Optical microscopy of the joint fracture surface (longitudinal section)

4. Discussion

The layer-by-layer additive manufacture is different from the traditional manufacture process in a unique manner characterized by local melting and directional thermal conduction, which results in all the differences in microstructure evolution and mechanical properties from the traditional wrought alloy.

4.1 WAAM process and thermal flow

The remelting boundary lines in Fig. 2b indicate the layer-by-layer building manner in the WAAM process: the transferred heat and mass from the arc and molten wire re-melt a certain amount of the previous layer and the liquid metal solidifies upon it to form a new layer.

In the layer-by-layer manufacture of the linear wall, the heat mostly flows from the top layer (where the weld pool is located) to the bottom. The orientation of the dendritic growth depends on the thermal gradient of the solidifying liquid and the solute enrichment of the liquid near the liquid-solid interface

[24,25]. Thus, from Fig. 2b, it can be seen that the dendrites grow perpendicular to the re-melting line and towards the top part since the heat was extracted towards the bottom/substrate in the WAAM process.

4.2 Transient aging effect

The inherent low aging temperature (482°C) of maraging steel is the decisive factor of the variation of microhardness, mechanical properties and precipitates formation of WAAM maraging steel along the building direction in the as deposited condition. Since the temperature of the weld pool of maraging steel is well above 1413°C, materials within some range near the weld pool can always be reheated up to reach such an aging temperature for a short duration. Due to the rapid aging response of the Al-Ti-hardened alloy, the accumulation of such durations will result in a transient aging effect to result in some extent of diffusion and precipitation to strengthen the material. However, this transient aging effect is not comparable to a proper aging due to the limited dwelling time and lack of constant temperature.

During the WAAM process, the transient thermal cycling from the successive deposits heat treats the previously deposited materials, thus the deposits closer to the bottom underwent numerous thermal cycles of a different magnitude to be aged more and gets harder than the top part. The uniformity of the microhardness after a proper aging (3 hrs at 482°C) heat treatment is due to the isotropically developed precipitation, which acts as a dislocation barrier in all directions [26]. It should be noticed that the topmost layer band is also the interface between the soft and the hard zones. As shown in Fig. 2a, there is a significant microhardness drop around first layer band (Zone A). Above this interface, the material cools down from the weld pool temperature, passes the austenitizing temperature zone and becomes entirely lath martensitic; due to the lack of successive thermal cycles, few precipitates are formed, and thus, the material is relatively softer.

During the deposition process, the top layer is heated well above the melting point (1413°C) at which the maraging steel was fully austenitic; after cooling down to room temperature, the structure transforms to fully martensitic in a supersaturated state with all the alloying elements remain in solid solution. In case of the successive layer depositions where the transient thermal cycles facilitate the diffusion, solute atoms diffuse out from the unit cell and form precipitates. The precipitates etch faster which is evident in the bottom part of the structure in the as deposited condition (as shown in Fig. 3a).

From the previous explanation, it can be inferred that different parts undergoing a different number of thermal cycles will have different amounts of intermetallic compounds precipitated: the more thermal cycles, the more precipitates. In the WAAM process, the as deposited material near the bottom part underwent more thermal cycles than the top, leading to more diffusion of solute atoms and formation of intermetallic compounds near the bottom part, which, however, was nowhere near to a controlled aging

treatment. After solution heat treatment, all solute atoms went into solution so the effect of thermal cycling was minimized and the actual aging time for the heat treated WAAM part was 3 hours. Considering that the 21-layer part was built within 1.5 hours, the real dwelling time near 482 °C was much less than 1.5 hours. Thus, the amount of precipitates of the top and bottom parts of the as deposited and heat treated structures should follow the sequence (less to more): as deposited top, as deposited bottom, heat treated top and bottom, which is verified in Fig. 7c. However, in Fig. 7c there are exceptions in the content of Fe_2Mo in the heat treated condition: the bottom part has noticeably less Fe_2Mo, and in the content of Ni_3Mo: the top part after a standard aging heat treatment has less Ni_3Mo than the bottom in the as deposited condition. It can thus be inferred that during heat treatment, the metastable Ni_3Mo could transfer to the more stable Fe_2Mo phase [14]. The difference of the Ni_3Ti content between the top and the bottom parts of the heat treated structure may result from the segregation of Ti element.

4.3 Explanation of the inferior mechanical properties

Apparently, the aging heat treatment of the WAAM maraging steel doesn't provide the strength increase as expected. Explanations are given as below.

4.3.1 Aging specification

From Table 3, the as deposited material possesses superior mechanical properties to the wrought maraging steel in the solutionized condition. However, after aging the WAAM material shows mechanical properties much lower than the wrought material, which indicates that the aging response of the WAAM maraging steel is not as profound as that of the wrought material.

The aging response critically depends on the microstructural condition of a component. The WAAM material has very different grain boundary structures from a wrought alloy and is lacking in initial compositional homogeneity. WAAM components are characterised by dendritic structures with low angle grain boundaries and segregation and thermal straining from the previously deposited layers due to successive deposition, whereas the wrought maraging steel features equiaxed grains with high grain boundaries.

In this study, the aging heat treatment used for a wrought alloy was applied to a WAAM structure, which may not be the optimum one for a WAAM component. More underpinning studies on the aging response for WAAM built structures need to be carried out. A possible solution could also be cold straining in between layer deposition to initiate re-crystallisation and thereby creating a structure comprises of high angle grain boundaries [34].

4.3.2 Wire composition and quality

The WAAM process is featured by melting the commercial welding wire to form the product. Therefore, all those in the wire go into the deposits including the alloying elements and the defects such as inclusions and porosities [3].

Maraging steels are precipitation hardened with Mo as the primary and Ti as the secondary hardener, hence having certain contents of such alloying elements in the as deposited material is the prerequisite of forming enough amount of intermetallic compounds to generate expected materials strengthening. However, three factors would affect the alloying elements content. Firstly, the chemical compositions of the wire and the wrought maraging steel are not identical (see Table 1). Secondly, the evaporation of alloying elements under the high-temperature electric arc will lead to element loss. Thirdly, when O is present, even in very low content, the higher affinity of Ti with O than with Ni leads to oxides formation and reduction of the amount of precipitates formed during age hardening.

Furthermore, the filler wire is one of the main sources of inclusions, nitrogen and oxygen; in the arc, inclusions can be vaporized and atomized to provide N and O to the weld pool and new inclusions will form through metallurgical reactions [2]. Fig. 13 shows the longitudinal section of the wire used in this research. A small amount of elongated inclusions is found in the wire. The EDS elemental analysis reveals that this is titanium nitride (as shown in Fig. 13 and Table 4), which is generated during the wire production process. It has been reported that the materials properties of maraging steels are greatly affected by the inclusion content, and TiN is one of the most commonly reported inclusions found in the wrought maraging steel. Severe grain boundary embrittlement will occur if Ti(C,N) is present at the grain boundary [35], resulting in a fast failure during the tensile test. Such influence is more noticeable in the aged condition when the material is more brittle [18]. Even though TiN was not detected in the WAAM maraging steel due to limited analysis in this research, it is reasonable to assume its presence in the WAAM material with the wire as the feedstock. Cleanness and purity are crucial for high strength steel to display its outstanding mechanical properties; therefore higher quality wire is required to produce WAAM maraging steel that can compete with the wrought material.

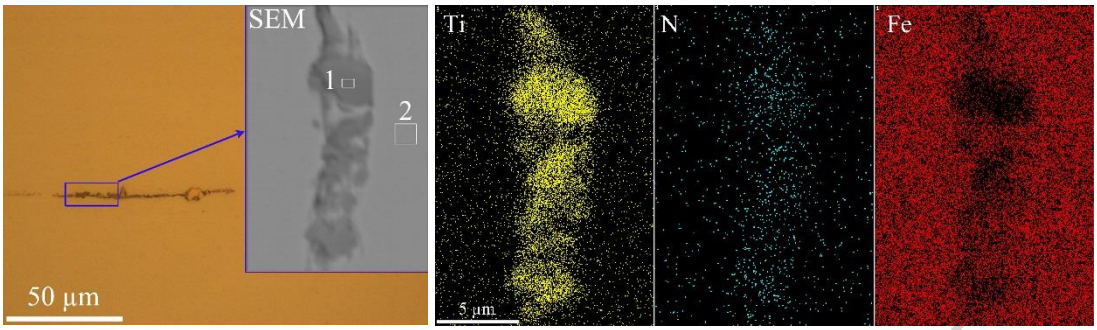

(a) optical microscopy (b) EDS elemental mapping

Fig. 13 Inclusions in the wire

Table 4. EDS elemental analysis of the inclusions (at. %)

	N	Ti	Fe	Rest (Co, Al, C, Si, Mn)
1	33.42	56.7	7.28	balance
2	-	0.53	69.42	balance

4.3.3 Austenite content

The soft austenite existing in the maraging steel has been reported to lower the strength of maraging steels as it doesn't harden during the aging heat treatment [36] and thus should be kept to minimum if high tensile strength is desired. The austenite in maraging steel consists of two sources: retained austenite and reverted austenite. The retained austenite forms when the material cools down from austenitizing temperature [37] while the reverted austenite forms mostly during the aging process by diffusion-controlled reaction [38]. The percentage of retained austenite in particular limits the usefulness of maraging steel as a high strength material [39].

In this paper, the austenite quantification is carried out using the direct comparison method based on the assumption that the integrated intensities of X-ray diffraction peaks for each phase are proportional to the volume fraction of that phase [40]. According to ASTM E975 standard, the volumetric fraction of austenite V_A is given as below,

$$V_A = \left(\frac{1}{q}\sum_{j=1}^{q} I_{Aj} / R_{Aj}\right) / \left[\left(\frac{1}{q}\sum_{j=1}^{q} I_{Aj} / R_{Aj}\right) + \left(\frac{1}{p}\sum_{i=1}^{p} I_{Mi} / R_{Mi}\right)\right] \quad (1)$$

Where *q* and *p* are the total number of austenite and martensite peaks respectively; *I* is the integrated intensity of a single diffraction peak; *R* is determined by the interplanar spacing (*hkl*), the Bragg angle *θ,* crystal structure and composition of the phase being measured. *R* can be calculated from basic principles.

Fig. 14 shows the XRD patterns for the top part of WAAM maraging steel under different conditions (as deposited, standard heat treated and solutionized) and for the heat treated wrought maraging steel. Table 5 summarises the corresponding austenite content. As can be seen, the diffractogram does not show any peaks of the intermetallic compounds under heat treated condition, which may be due to the low phase content (less than 5% [14]) and the very dispersed distribution [39]. The top part in the as deposited condition does not undergo successive thermal cycles, thus only tiny austenite peaks are observed in the diffractogram; in contrast, more austenite peaks are found at the same position after the standard heat treatment, indicating larger amount of austenite forming (13.1% versus 8.3%). Solutionizing eliminates the elemental segregation, which helps reduce the austenite amount compared to the as deposited condition (2.1% versus 8.3%). However, the wrought maraging steel hardly contains austenite even under heat treated condition, which might be due to the different microstructure from the WAAM part. The different microstructure leads to a different response to elements segregation and austenite formation, which is one of the major issues weakening the mechanical properties of WAAM maraging steels.

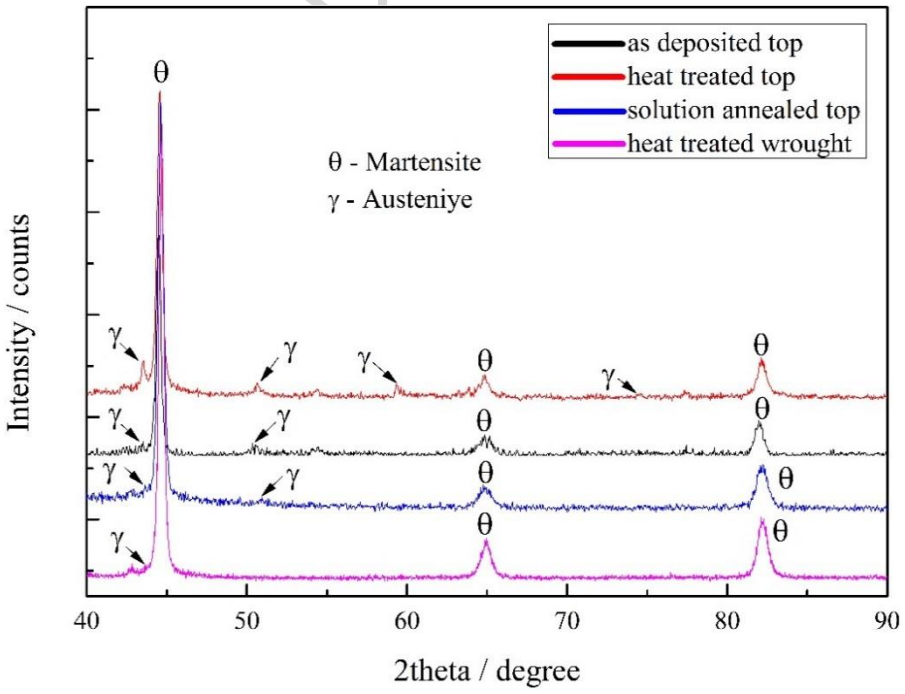

Fig. 14. X-ray diffractogram of the maraging steel

Table 5. Volumetric fraction of the austenite (%)

	Austenite γ	Martensite θ
Heat treated wrought	0.94	99.06
Solutionized top	2.1	97.9
As deposited top	8.3	91.7
Heat treated top	13.1	86.9

5. Conclusions

The WAAM process has been applied to produce defect-free and full dense maraging steel components. In the as deposited condition, the microstructure features uniformly distributed layer bands and upwards dendritic growth perpendicular to the remelting line; the mechanical properties show slight anisotropy with the vertical direction lower than the horizontal, yet both of them are superior to that of solutionized wrought material. However, the properties are not uniform with the softer material at the top in the region where less thermal cycles have been experienced and less intermetallic compounds are precipitated, as indicated by the microhardness measurements and EBSD phase statistics results. A standard solution + aging heat treatment designed for the wrought 250-grade maraging steel has been applied to WAAM maraging steel, which eliminates the microstructural heterogeneity from the bottom to the top and gives an increase in strength of 24.7% (this is still not quite as high as the heat treated wrought alloy). More austenites are detected after heat treatment, which is promoted by the segregation of Mo and Ti. The low angle columnar grains dominated WAAM material shows less pronounced response to aging heat treatment and better accommodation to the retained and reverted austenite compared to the equiaxed grain dominated wrought alloy, which is the main reason for lower mechanical properties attained. Besides, the wire quality (TiN inclusions) should also be considered if higher mechanical properties are to be achieved. Future studies will be conducted to create a more tailored heat treatment cycle for the WAAM materials and investigate intermediate cold working in order to create the microstructure with higher angle grain boundary to further increase the mechanical properties.

Acknowledgements

The authors wish to acknowledge the financial support from China Scholarship Council (NO. 201506680057) and the WAAMMat programme industrial partners. The authors would like to thank Dr. Xianwei Liu for the assistance during the SEM and EBSD analysis and metallurgist Armando Caballero and Miss. Qiong Gao for the helpful discussion during the microstructural analysis.

References

[1] B. Cong, J. Ding, S. Williams, Effect of arc mode in cold metal transfer process on porosity of additively manufactured Al-6.3%Cu alloy, Int. J. Adv. Manuf. Technol. 76 (2014) 1593–1606. doi:10.1007/s00170-014-6346-x.

[2] J. Gu, J. Ding, S.W. Williams, H. Gu, P. Ma, Y. Zhai, The effect of inter-layer cold working and post-deposition heat treatment on porosity in additively manufactured aluminum alloys, J. Mater. Process. Technol. 230 (2016) 26–34. doi:10.1016/j.jmatprotec.2015.11.006.

[3] S.W. Williams, F. Martina, A.C. Addison, J. Ding, G. Pardal, P. Colegrove, Wire+Arc Additive Manufacturing, Mater. Sci. Technol. 0 (2015) 1–7. doi:10.1179/1743284715Y.0000000073.

[4] F. Martina, J. Mehnen, S.W. Williams, P. Colegrove, F. Wang, Investigation of the benefits of plasma deposition for the additive layer manufacture of Ti-6Al-4V, J. Mater. Process. Technol. 212 (2012) 1377–1386. doi:10.1016/j.jmatprotec.2012.02.002.

[5] J. Gu, J. Ding, S.W. Williams, H. Gu, J. Bai, Y. Zhai, P. Ma, The strengthening effect of inter-layer cold working and post-deposition heat treatment on the additively manufactured Al– 6.3Cu alloy, Mater. Sci. Eng. A. 651 (2016) 18–26. doi:10.1016/j.jmatprotec.2015.11.006.

[6] B. Cong, R. Ouyang, B. Qi, J. Ding, Influence of Cold Metal Transfer Process and Its Heat Input on Weld Bead Geometry and Porosity of Aluminum-Copper Alloy Welds, Rare Met. Mater. Eng. 45 (2016) 606–611. doi:10.1016/S1875-5372(16)30080-7.

[7] T. Skiba, B. Baufeld, O. Van Der Biest, Microstructure and Mechanical Properties of Stainless Steel Component Manufactured by Shaped Metal Deposition, ISIJ Int. 49 (2009) 1588–1591. doi:10.2355/isijinternational.49.1588.

[8] B. Baufeld, Mechanical properties of INCONEL 718 parts manufactured by shaped metal deposition (SMD), J. Mater. Eng. Perform. 21 (2012) 1416–1421. doi:10.1007/s11665-011-0009-y.

[9] J. Ding, P. Colegrove, F. Martina, S. Williams, R. Wiktorowicz, M.R. Palt, Development of a laminar flow local shielding device for wire+arc additive manufacture, J. Mater. Process. Technol. 226 (2015) 99–105. doi:10.1016/j.jmatprotec.2015.07.005.

[10] J. An, F. Meng, X. Lv, H. Liu, X. Gao, Y. Wang, Y. Lu, Improvement of mechanical properties of stainless maraging steel laser weldments by post-weld ageing treatments, Mater. Des. 40 (2012)

276–284. doi:10.1016/j.matdes.2012.03.020.

[11] Y. Li, W. Yan, J.D. Cotton, G.J. Ryan, Y. Shen, W. Wang, Y. Shan, A new 1 . 9 GPa maraging stainless steel strengthened by multiple precipitating species, J. Mater. 82 (2015) 56–63. doi:10.1016/j.matdes.2015.05.042.

[12] V. Rajkumar, N. Arivazhagan, Role of pulsed current on metallurgical and mechanical properties of dissimilar metal gas tungsten arc welding of maraging steel to low alloy steel, J. Mater. 63 (2014) 69–82. doi:10.1016/j.matdes.2014.05.055.

[13] O. Moshka, M. Pinkas, E. Brosh, V. Ezersky, L. Meshi, Addressing the issue of precipitates in maraging steels - Unambiguous answer, Mater. Sci. Eng. A. 638 (2015) 232–239. doi:10.1016/j.msea.2015.04.067.

[14] J.M. Pardal, S.S.M. Tavares, M.P. Cindra Fonseca, H.F.G. Abreu, J.J.M. Silva, Study of the austenite quantification by X-ray diffraction in the 18Ni-Co-Mo-Ti maraging 300 steel, J. Mater. Sci. 41 (2006) 2301–2307. doi:10.1007/s10853-006-7170-y.

[15] ASM International, ASM Handbook: Volume 1 Properties and selection: irons steels and high performance alloys, 10th ed., ASM International, Materials Park, Ohio, 2001. doi:10.1016/S0026-0576(03)90166-8.

[16] S.L. Campanelli, A. Angelastro, C.G. Signorile, G. Casalino, Investigation on direct laser powder deposition of 18 Ni (300) marage steel using mathematical model and experimental characterisation, Int. J. Adv. Manuf. Technol. 89 (2017) 885–895. doi:10.1007/s00170-016-9135-x.

[17] L. Thijs, J. Van Humbeeck, K. Kempen, E. Yasa, J.-P. Kruth, Investigation on the inclusions in maraging steel produced by Selective Laser Melting, in: 5th Int. Conf. Adv. Res. Virtual Rapid Prototyp., 2011: pp. 297–304. doi:doi:10.1201/b11341-48\r10.1201/b11341-48.

[18] K. Kempen, E. Yasa, L. Thijs, J.P. Kruth, J. Van Humbeeck, Microstructure and mechanical properties of selective laser melted 18Ni-300 steel, Phys. Procedia. 12 (2011) 255–263. doi:10.1016/j.phpro.2011.03.033.

[19] S.L. Campanelli, N. Contuzzi, A.D. Ludovico, Manufacturing of 18 Ni Marage 300 Steel Samples by Selective Laser Melting, Adv. Mater. Res. 83–86 (2009) 850–857. doi:10.4028/www.scientific.net/AMR.83-86.850.

[20] E. Yasa, K. Kempen, J. Kruth, Microstructure and mechanical properties of Maraging Steel 300 after selective laser melting, in: Proc. 21st Int. Solid Free. Fabr. Symp., 2010: pp. 383–396. http://utwired.engr.utexas.edu/lff/symposium/proceedingsArchive/pubs/Manuscripts/2010/2010-32-Yasa.pdf.

[21] G. Casalino, S.L. Campanelli, N. Contuzzi, A.D. Ludovico, Experimental investigation and statistical optimisation of the selective laser melting process of a maraging steel, Opt. Laser Technol. 65 (2015) 151–158. doi:10.1016/j.optlastec.2014.07.021.

[22] T. Arai, Volume 4: Heat Treating, in: ASM Handb., ASM International, 1991: p. 2173. doi:10.1016/S0026-0576(03)90166-8.

[23] F.H. Lang, N. Kenyon, Welding of Maraging Steels, 1971.

[24] J.D. Hunt, Steady state columnar and equiaxed growth of dendrites and eutectic, Mater. Sci. Eng. 65 (1984) 75–83. doi:10.1016/0025-5416(84)90201-5.

[25] I. Yadroitsev, P. Krakhmalev, I. Yadroitsava, P. Bertrand, I. Smurov, Energy input effect on the microstructure, morphology and stability of single track from metallic powder in selective laser melting, J. Mater. Process. Technol. 213 (2013) 606–613. doi:http://dx.doi.org/10.1016/j.jmatprotec.2012.11.014.

[26] K.J.A. Brookes, Maraging steel for additive manufacturing - Philipp Stoll's paper at DDMC 2016, Met. Powder Rep. 71 (2016) 149–152. doi:10.1016/j.mprp.2016.04.087.

[27] S.D. Meshram, G. Madhusudhan Reddy, S. Pandey, Friction stir welding of maraging steel (Grade-250), Mater. Des. 49 (2013) 58–64. doi:10.1016/j.matdes.2013.01.016.

[28] C.R. Shamantha, R. Narayanan, K.J.L. Iyer, V.M. Radhakrishnan, S.K. Seshadri, S. Sundararajan, S. Sundaresan, Microstructural changes during welding and subsequent heat treatment of 18Ni (250-grade) maraging steel, Mater. Sci. Eng. A. 287 (2000) 43–51. doi:10.1016/S0921-5093(00)00838-8.

[29] J.M. Pardal, S.S.M. Tavares, V.F. Terra, M.R. Da Silva, D.R. Dos Santos, Modeling of precipitation hardening during the aging and overaging of 18Ni-Co-Mo-Ti maraging 300 steel, J. Alloys Compd. 393 (2005) 109–113. doi:10.1016/j.jallcom.2004.09.049.

[30] S.P. Sagar, N. Parida, S. Das, R.N. Ghosh, Precipitation Hardening Study of Ageing of Maraging Steel Using Ultrasonic Technique, Mater. Sci. (2006) 7–8.

[31] E.A. Jägle, P.-P. Choi, J. Van Humbeeck, D. Raabe, Precipitation and austenite reversion behavior of a maraging steel produced by selective laser melting, J. Mater. Res. 29 (2014) 2072. doi:10.1557/jmr.2014.204.

[32] J. Millán, S. Sandlöbes, A. Al-Zubi, T. Hickel, P. Choi, J. Neugebauer, D. Ponge, D. Raabe, Designing Heusler nanoprecipitates by elastic misfit stabilization in Fe-Mn maraging steels, Acta Mater. 76 (2014) 94–105. doi:10.1016/j.actamat.2014.05.016.

[33] ASTM, Standard Specification for Superstrength Alloy Steel Forgings 1, Astm. (2015) 1–7. doi:10.1520/A0579.

[34] P. a. Colegrove, H.E. Coules, J. Fairman, F. Martina, T. Kashoob, H. Mamash, L.D. Cozzolino, Microstructure and residual stress improvement in wire and arc additively manufactured parts through high-pressure rolling, J. Mater. Process. Technol. 213 (2013) 1782–1791. doi:10.1016/j.jmatprotec.2013.04.012.

[35] P. Würzinger, R. Rabitsch, W. Meyer, Production of maraging steel grades and the influence of specified and nonspecified elements for special applications, J. Mater. Sci. 39 (2004) 7295–7302. doi:10.1023/B:JMSC.0000048744.03279.ec.

[36] F.H. Lang, N. Kenyon, Welding of Maraging Steels, Weld. Res. Concil. (1971) 41.

[37] B. AlMangour, J.M. Yang, Improving the surface quality and mechanical properties by shot-peening of 17-4 stainless steel fabricated by additive manufacturing, Mater. Des. 110 (2016) 914–924. doi:10.1016/j.matdes.2016.08.037.

[38] E.A. Jägle, P. Choi, J. Van Humbeeck, D. Raabe, Precipitation and austenite reversion behavior of a maraging steel produced by selective laser melting, J. Mater. Res. 29 (2014) 2072. doi:10.1557/jmr.2014.204.

[39] I. Journal, O.F. Advanced, H. Ahmed, H. Central, Evaluation of Relatively Low Strength Maraging Evaluation of Relatively Low Strength Maraging Steel, (2015).

[40] Astm, Standard Practice for X-Ray Determination of Retained Austenite in Steel with Near Random Crystallographic Orientation 1, Astm. 3 (2009) 1–7. doi:10.1520/E0975-13.necessary.

Figure captions

Tables

Table 1. Chemical composition of the MARVAL 18S wire, maraging 200 and 250-grade steel (wt. %)

	Ni	Mo	Co	Ti	Al	C	Fe
Wire [a]	18.28	4.69	8.21	0.44	0.11	<0.01	Balance
18Ni (200) [15]	18	3.3	8.5	0.2	0.1	<0.03	Balance
18Ni (250) [b]	18.3	4.8-4.9	7.7	0.5	0.07-0.08	0.004	Balance

[a] *from data sheet of the wire package*

[b] *from date sheet provided by Smiths Metal Centres*

Table 2. EDS elemental analysis of the austenite and martensitic matrix (wt. %)

	Ti	Mo	Ni	Co	Rest (Fe, Al, C)
C	1.39	5.16	19.85	8.89	balance
D	0.08	3.09	17.41	8.38	balance
wire	0.44	4.69	18.28	8.21	balance

Table 3. Summary of mechanical properties of maraging steel

		UTS /MPa	0.2%YS /MPa	Elongation /%
as deposited	WAAM (horizontal)	1118±94	904±78	11.7±0.8
	WAAM (vertical)	1026±10	833±26	8.0±3.8
unaged	Wrought 200 [15]	965-1000	760-807	17-18
	Wrought 250 [15]	1000-1140	725-895	8-16
aged	WAAM (horizontal)	1410±32	1303±29	8.5±3.3
	WAAM (vertical)	1345±19	1227±31	6.0±1.7
	Wrought 200 [33]	1450	1380	12
	Wrought 250 [33]	1760	1720	10

Table 4. EDS elemental analysis of the inclusions (at. %)

	N	Ti	Fe	Rest (Co, Al, C, Si, Mn)
1	33.42	56.7	7.28	balance
2	-	0.53	69.42	balance

Table 5. Volumetric fraction of the austenite (%)

	Austenite γ	Martensite θ
Heat treated wrought	0.94	99.06
Solutionized top	2.1	97.9
As deposited top	8.3	91.7
Heat treated top	13.1	86.9

Graphical Abstract

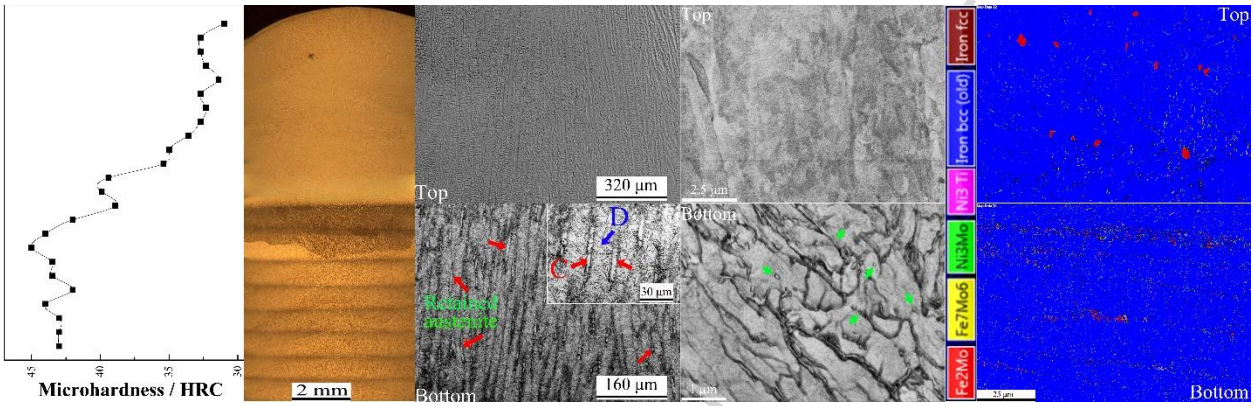

Highlights

- Wire + arc additive manufacture (WAAM) was applied to produce maraging steel structures.
- Microstructure evolution of WAAM alloy was characterized and correlated with the layer-by-layer building manner.
- Mechanical properties of WAAM alloy were tested and correlated with the aging response of WAAM microstructure.
- Retained austenite content was measured and correlated with the tensile strength loss.

2017-12-06

Microstructural evolution and mechanical properties of maraging steel produced by wire + arc additive manufacture process

Xu, Xiangfang

Elsevier

Xu X, Ganguly S, Ding J, Huo S, Williams S, Martina F, Microstructural evolution and mechanical properties of maraging steel produced by wire + arc additive manufacture process, Materials Characterization, Volume 143, September 2018, Pages 152-162

http://dx.doi.org/10.1016/j.matchar.2017.12.002